Li^+ Extraction/Insertion Reactions with $LiZn_{0.5}Mn_{1.5}O_4$ Spinel in the Aqueous Phase

Qi Feng,* Hirofumi Kanoh, Yoshitaka Miyai, and Kenta Ooi

Shikoku National Industrial Research Institute, 2217-14 Hayashi-cho Takamatsu-shi Kagawa 761-03, Japan

Received September 13, 1994. Revised Manuscript Received December 5, 1994[⊗]

Spinel-type lithium–zinc–manganese oxide $(Li_{0.5}Zn_{0.5})[Li_{0.5}Mn_{1.5}]O_4$ was prepared by a coprecipitation/thermal crystallization method. The Li^+ extraction/insertion reactions with the spinel in the aqueous phase were investigated by X-ray diffraction, DTA-TG analyses, FT-IR spectroscopy, pH titration, and distribution coefficient (K_d) measurement. The Li^+ extraction and insertion proceed by topotactic ion-exchange-type mechanisms. The Zn^{2+} at the tetrahedral sites caused a decrease in the extractabilities of Li^+ during acid treatment. The spinel with ordered arrangement of Li^+ and Zn^{2+} at 8a tetrahedral sites showed a markedly lower Li^+ extractability than the spinel with random arrangement of Li^+ and Zn^{2+} at the same sites. The inhibiting effect of Zn^{2+} on Li^+ extractability was discussed in terms of the Li^+ migration pathway in the spinel structure. The Li^+-extracted sample showed a lithium ion-sieve property from microamount to macroamount of metal ion loading.

Introduction

Spinel-type lithium–manganese oxides are an interesting class of materials. Li^+ can be extracted/inserted topotactically from/into the oxides by electrochemical or chemical methods.[1,2] A large number of studies on the Li^+ extraction/insertion reactions have been carried out in the organic phase with a view to developing nonaqueous lithium rechargeable batteries.[3–9] Studies on Li^+ extraction/insertion reactions in the aqueous phase have been carried out with a view to developing a Li^+ adsorbent for a dilute solution.[10–16] The spinel-type lithium-manganese oxides show a specific selectivity for the adsorption of Li^+ among alkali, alkaline earth, and transition-metal ions after topotactic extraction of Li^+ with an acid.[10–21] The selection properties can be explained on the basis of the ion-sieve effect of the spinel lattice which has a three-dimensional tunnel suitable in size for fixing lithium ions.

We have studied the mechanism of Li^+ extraction/insertion reactions with spinel-type lithium–manganese oxides in aqueous solution.[22,23] There are two types of extraction/insertion reactions: one is a redox-type and the other an ion-exchange type. The Li^+ extraction/insertion sites can be classified into redox-type and ion-exchange-type sites. The numbers of the redox-type and ion-exchange-type sites correlate well with the amounts of trivalent Mn ions and the defects of Mn ions in the original lithium-manganese oxide spinels, respectively.[22]

For developing an ion-exchange-type Li^+ absorbent, $(Li)[Mg_{0.5}Mn_{1.5}]O_4$, $(Li)[AlMn]O_4$, and $(Li_{0.6}Fe_{0.4})[Li_{0.4}Fe_{0.6}Mn]O_4$ spinels (( ) and [ ] are 8a tetrahedral sites and 16d octahedral sites of the spinel structure, respectively) have been synthesized by doping the third metal ions (Mg^{2+}, Al^{3+}, and Fe^{3+}) into the lithium–manganese oxide.[24,25] These spinels show ion-exchange properties in the Li^+ extraction/insertion processes, because most of the manganese in the spinels is tetravalent.

The present paper describes fundamental studies on the Li^+ extraction/insertion reactions with the $(Li_{0.5}Zn_{0.5})[Li_{0.5}Mn_{1.5}]O_4$ spinel in an aqueous phase. The effect of the cation arrangement of the spinel on the extraction/insertion reactions is discussed.

Experimental Section

Sample Preparation. The lithium–zinc–manganese oxides were prepared by a coprecipitation/thermal crystallization

[⊗] Abstract published in *Advance ACS Abstracts,* December 15, 1994.

(1) Goodenough, J. B.; Thackeray, M. M.; David, W. I. F.; Bruce, P. G. *Rev. Chim. Miner.* **1984**, *21*, 435.
(2) Hunter, J. C. *J. Solid State Chem.* **1981**, *39*, 142.
(3) Thackeray, M. M.; David, W. I. F.; Bruce, P. G.; Goodenough, J. B. *Mater. Res. Bull.* **1983**, *18*, 461.
(4) Thackeray, M. M.; Johnson, P. J.; Picciotto, L. A. D.; David, W. I. F.; Bruce, P. G.; Goodenough, J. B. *Mater. Res. Bull.* **1984**, *19*, 179.
(5) Rossouw, M. H.; Kock, A. De.; Picciotto, L. A. De.; Thackeray, M. M.; David, W. I. F.; Ibberson, R. M. *Mater. Res. Bull.* **1990**, *25*, 173.
(6) Ohzuku, T.; Kitagawa, M.; Hirai, T. *J. Electrochem. Soc.* **1990**, *137*, 40.
(7) Li, L.; Pistoia, G. *Solid State Ionics* **1991**, *47*, 231.
(8) Guyomard, D.; Tarascon, J. M. *J. Electrochem. Soc.* **1992**, *139*, 937.
(9) Shokoohi, F. K.; Tarascon, J. M.; Wilkens, B. J.; Guyomard, D.; Change, C. C. *J. Electrochem. Soc.* **1992**, *139*, 1845.
(10) Vol'khin, V. V.; Leont'eva, G. V.; Onolin, S. A. *Neorg. Mater.* **1973**, *6*, 1041.
(11) Leont'eva, G. V.; Chirkova, L. G. *Zh. Prikl. Khin.* **1988**, *61*, 734.
(12) Shen, X. M.; Clearfield, A. *J. Solid State Chem.* **1986**, *64*, 270.
(13) Ooi, K.; Miyai, Y.; Katoh, S. *Sep. Sci. Technol.* **1986**, *21*, 755.
(14) Ooi, K.; Miyai, Y.; Katoh, S. *Sep. Sci. Technol.* **1987**, *22*, 1779.
(15) Ooi, K.; Miyai, Y.; Katoh, S. *Solvent Extr. Ion Exch.* **1987**, *5*, 561.
(16) Ooi, K.; Miyai, Y.; Katoh, S. Maeda, H.; Abe, M. *Bull. Chem. Soc. Jpn.* **1988**, *61*, 407.
(17) Ooi, K.; Miyai, Y.; Katoh, S. Maeda, H.; Abe, M. *Chem. Lett.* **1988**, 989.
(18) Ooi, K.; Miyai, Y.; Katoh, S. Maeda, H.; Abe, M. *Langmuir* **1989**, *5*, 150.
(19) Ooi, K.; Miyai, Y.; Katoh, S. Maeda, H.; Abe, M. *Langmuir* **1990**, *6*, 289.
(20) Miyai, Y.; Ooi, K.; Katoh, S. *Sep. Sci. Technol.* **1988**, *23*, 179.
(21) Miyai, Y.; Ooi, K.; Katoh, S. *J. Colloid Interface Sci.* **1989**, *130*, 5251.
(22) Feng, Q.; Miyai, Y.; Kanoh, H.; Ooi, K. *Langmuir 1992*, *8*, 1861.
(23) Ooi, K.; Miyai, Y.; Sakakihara, J. *Langmuir* **1991**, *7*, 1167.
(24) Feng, Q.; Miyai, Y.; Kanoh, H.; Ooi, K. *Chem.* Mater. **1993**, *5*, 311.
(25) Liu, Y. F.; Feng, Q.; Ooi, K. *J. Colloid Interface Sci.* **1994**, *163*, 130.

0897-4756/95/2807-0379$09.00/0

method. A solution of 1 M (1 M = 1 mol/L) LiOH was poured into a mixed solution (100 mL) of $Mn(NO_3)_2$ (0.3 M) and $Zn(NO_3)_2$ (0.1 M). After the pH of the original solution reached 10.5, the precipitate was filtered and washed with water. A solution (100 mL) of 0.2 M LiOH was added to the precipitate (Li:Mn mole ratio = 2:3), boiled at 100 °C for 4 h, air-dried at 80 °C, and then heat-treated in air for 8 h at 400, 500, 600, and 800 °C, respectively. The samples were designated as Zn-400, Zn-500, Zn-600, and Zn-800, where the numbers represent heating temperatures.

Li^+ Extraction/Insertion Reactions. Li^+ extraction and insertion were investigated at room temperature. In the extraction study, lithium–zinc–manganese oxide (10 g) was treated with a HNO_3 solution (1 L) for 2 days to obtain the acid-treated sample. The concentration of HNO_3 varied over a range between 0.1 and 10 M. The sample was filtered, washed with water, and air-dried at 70 °C. The concentrations of Li, Zn, and Mn in the supernatant solution were determined by atomic absorption spectroscopy. The extractabilities of the metal ions by the acid treatment were calculated from these concentrations. The samples obtained by three acid treatments of Zn-600 and Zn-400 with 2 M HNO_3 were designated as Zn-600(H) and Zn-400(H), respectively.

In the insertion study, the acid-treated sample (Zn-600(H) or Zn-400(H), 2 g) was immersed in a 0.1 M LiOH solution (500 mL) for 7 days to obtain a Li^+-inserted sample. The sample was filtered, washed with water, and air-dried at 70 °C. The Li^+-inserted samples were designated as Zn-600(Li) and Zn-400(Li), respectively.

Chemical Analyses. The lithium, zinc, and manganese contents of the oxide samples were determined after dissolving them with a mixed solution of H_2SO_4 and H_2O_2. Lithium and zinc concentrations were determined by atomic absorption spectrometry, and manganese concentration by absorption spectrometry at 523 nm after oxidizing Mn to Mn(VII) with $(NH_4)_2S_2O_8$. The available oxygen of each sample was determined by the standard oxalic method.[26] The mean oxidation number (Z_{Mn}) of manganese was evaluated from the value of available oxygen and the manganese content.

Physical Analyses. X-ray analysis was carried out on a Rigaku type RINT1200 X-ray diffractometer with a graphite monochromator. The mechanical deviation of diffraction angles was corrected by scanning the whole-angle range with silicon powder. Infrared spectra were obtained by the KBr method on a Model JTR–RFX3001 JEOL infrared spectrometer. DTA-TG curves were obtained on a MAC Science thermal analyzer (System 001, TG-DTA 2000) at a heating rate of 10 °C/min.

pH Titration. A 0.1-g portion of each acid-treated sample was immersed in a mixed solution (10 mL) of (0.1 M MCl + MOH, M = Li, Na) in varying ratios with intermittent shaking at 25 °C. After the sample was shaken for 7 days, the pH of the supernatant solution was determined with a Horiba Model M8s pH meter.

Distribution Coefficient (K_d). The K_d values of the alkali metal ions were determined by a batch method. The acid-treated sample (0.1 g) was immersed in a solution (10 mL) containing 5×10^{-4} M each of Li^+, Na^+, K^+, Rb^+, and Cs^+ at pH 2. After attaining equilibrium (for 14 days), the metal ion concentrations in the supernatant solution were determined by atomic absorption spectrometry. The metal ion uptakes were calculated from the concentrations relative to the initial concentrations in the solution. The K_d values were calculated using the following equation:

$$K_d\ (\text{mL/g}) = \frac{\text{metal ion uptake (mg/g of sample)}}{\text{metal ion concentration (mg/mL solution)}}$$

Results and Discussion

Preparation and Characterization of Lithium–Zinc–Manganese Oxide. X-ray diffraction studies on the heat-treated samples show that the pure spinel phase is formed in a temperature range between 400 and 600 °C (Figure 1). A small amount of monoclinic phase (Li_2MnO_3) is formed in addition to the spinel phase when the heating temperature is higher than 600 °C. The diffraction peaks become stronger and sharper with increasing heating temperature. The Zn-400 spinel shows the X-ray diffraction pattern of a face-centered cubic crystal system (space group $Fd3m$). The presence of (220) and (422) reflection peaks indicates the spinel with Zn at the 8a tetrahedral sites and Mn at the 16d octahedral sites of a cubic closed-packed oxygen framework.[27] The cation distribution of Zn-400 can be written as $(Li_{0.5}Zn_{0.5})[Li_{0.5}Mn_{1.5}]O_4$. The X-ray pattern of the Zn-600 spinel agrees well with that for $LiZn_{0.5}Mn_{1.5}O_4$ (ASTM 32–0610). This spinel has a superstructure; it shows some new reflection peaks in addition to the peaks of Zn-400, owing to ordered arrangements of Li and Zn at the 8a tetrahedral sites and Li and Mn at the 16d octahedral sites.[28] The spinel structure with cation ordered arrangement is shown in Figure 2. The crystal system of the spinel belongs to a primitive cubic system (space group $P4_332$). The crystal symmetry is decreased, owing to the cation ordering.

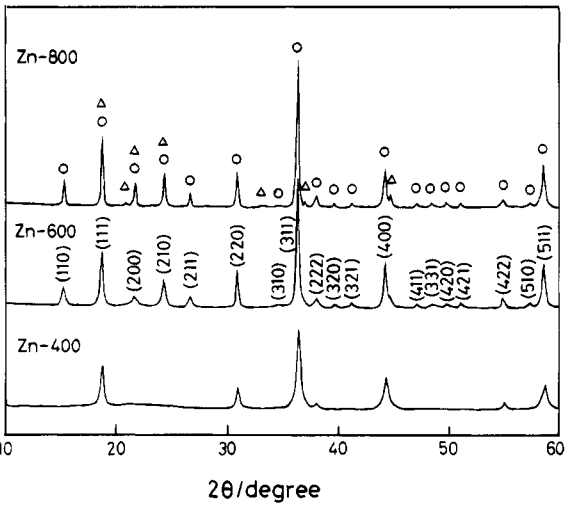

Figure 1. X-ray diffraction patterns of lithium–zinc–manganese oxides prepared at different temperatures. ○, peaks corresponding to spinel phase; △, peaks corresponding to monoclinic phase.

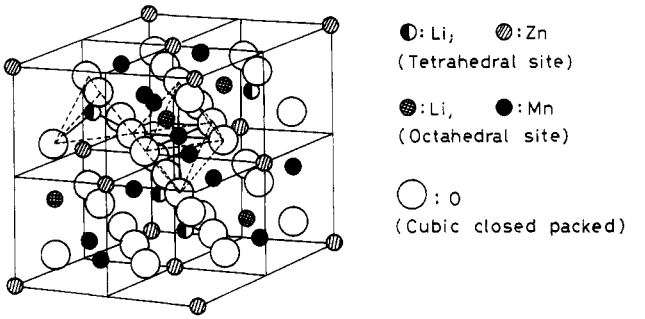

Figure 2. Structure of $(Li_{0.5}Zn_{0.5})[Li_{0.5}Mn_{1.5}]O_4$ with ordered arrangement of cations (space group $P4_332$).

Chemical analysis results for Zn-600 and Zn-400 are summarized in Table 1. Mean oxidation numbers of Mn (Z_{Mn}) are close to 4, indicating that most of the manganese ions are in a tetravalent state in both the

(26) Japan Industrial Standard (JIS), 1969, M8233.

(27) Wickham, D. G.; Croft, W. *J. Phys. Chem. Solid* **1958**, 7, 351.
(28) Blasse, G. *Philips Res. Rpts.*; Eindhoven, 1964; Suppl. No. 3.

Table 1. Compositional and Structural Parameters of Original, Acid-Treated, and Li^+-Inserted Samples[a]

sample	a_0 (Å)	Z_{Mn}	Li/Mn	Zn/Mn	H/Mn	formula
original						
Zn-600	8.20	3.99	0.614	0.328		$Li_{0.93}Zn_{0.50}Mn_{1.51}O_4$
Zn-400	8.17	4.01	0.634	0.339		$Li_{0.95}Zn_{0.51}Mn_{1.50}O_4$
acid-treated						
Zn-600(H)	8.18	4.01	0.344	0.264	0.35	$Li_{0.53}H_{0.54}Zn_{0.40}Mn_{1.53}O_4$
Zn-400(H)	8.14	4.04	0.034	0.210	0.89	$Li_{0.05}H_{1.33}Zn_{0.31}Mn_{1.49}O_4$
Li^+-inserted						
Zn-600(Li)	8.20	4.00	0.460	0.270	0.22	$Li_{0.70}H_{0.33}Zn_{0.41}Mn_{1.53}O_4$
Zn-400(Li)	8.17	4.01	0.469	0.215	0.34	$Li_{0.71}H_{0.52}Zn_{0.33}Mn_{1.52}O_4$

[a] a_0: lattice constant of spinel structure. Z_{Mn}: mean oxidation number of manganese.

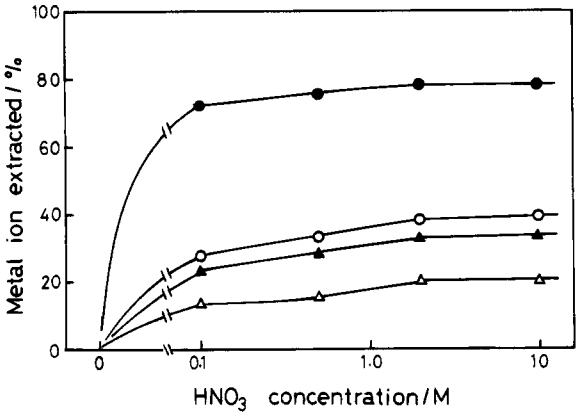

Figure 3. Effect of HNO_3 concentration on the extractability of lithium ion (▲, ●) and zinc ion (△, ○) from lithium–zinc–manganese oxides. ▲, △: Zn-600; ●, ○: Zn-400.

samples. The Li/Mn and Zn/Mn mole ratios are close to the theoretical values derived from the chemical formula of $LiZn_{0.5}Mn_{1.5}O_4$. The chemical formulas of Zn-600 and Zn-400 can be evaluated from the compositional data using the condition of electroneutrality (Table 1).[24]

Acid Treatment of Original Samples. The extractabilities of Li^+, Zn^{2+}, and Mn^{2+} ions from the Zn-600 and Zn-400 were investigated by using HNO_3 solutions with different concentrations. The extractabilities of Li^+ and Zn^{2+} become constants when the HNO_3 concentration is higher than 2 M (Figure 3). They are greatly dependent on the temperature of the heat treatment, increasing with decreasing temperature. The Li^+ and Zn^{2+} extractabilities are 95% and 40% for Zn-400 and 44% and 20% for Zn-600, respectively, when they are acid-treated with a 2 M HNO_3 solution three times. Manganese dissolutions were less than 2% for each samples during the acid treatment. These results indicate that Li^+ and Zn^{2+} are selectively extracted from the heat-treated samples. The manganese dissolutions are due to disproportion of a small amount of Mn(III) to Mn(IV) and Mn(II) (Mn(III) → $^1/_2$Mn(IV) + $^1/_2$Mn(II)), corresponding to the redox-type extractions of Li^+ and Zn^{2+}.[2,18,22,24] Proportion of the redox-type extraction is less than 5%, which can be estimated from the amount of dissoved Mn.[22,24]

Compositional analysis of the acid-treated samples (Zn-600(H) and Zn-400(H)) indicates that the lithium and zinc contents (Li/Mn and Zn/Mn) decrease, but the lattice proton content (H/Mn which was obtained from DTA-TG analysis described below) increases with the acid treatment (Table 1). The H/Mn values of the acid-treated samples agreed well with the total amounts of

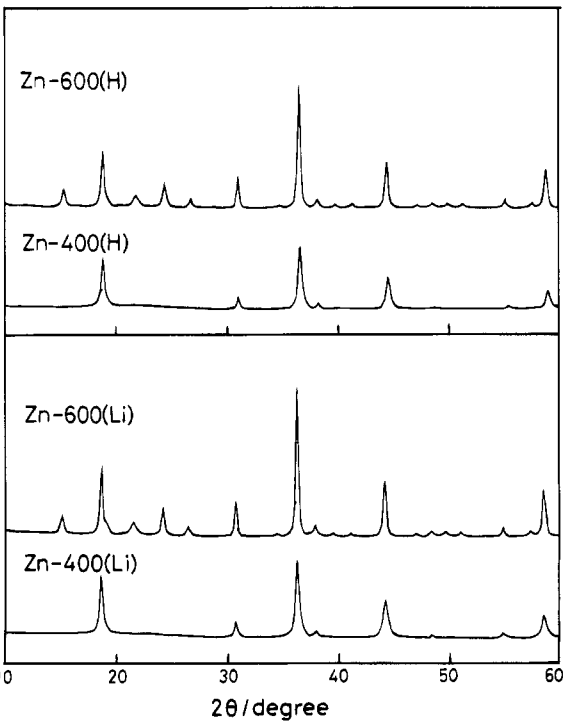

Figure 4. X-ray diffraction patterns of the acid-treated (top) and Li^+-inserted (bottom) samples.

extracted Li^+ and Zn^{2+} (0.40 equiv/Mn for Zn-600 and 0.86 equiv/Mn for Zn-400). This indicates that Li^+ and Zn^{2+} are nearly stoichiometrically extracted by the Li^+/H^+ and Zn^{2+}/H^+ ion-exchange reactions. Z_{Mn} remains almost constant (at around 4) after the acid treatment, indicating the rare presence of the redox-type reaction in the extraction process. The compositional formulas of the acid-treated samples can be derived from the compositional analysis data using the condition of electroneutrality;[24] the formulas are given in Table 1.

Physical Properties of the Acid-Treated Samples. The X-ray diffraction patterns of the acid-treated samples showed that the spinel structure remained after the Li^+ extraction (Figure 4 top), but the lattice constants decreased slightly (Table 1). This indicates that the Li^+ extraction reaction proceeds topotactically.

The DTA-TG curves for sample Zn-600(H) show endothermic peaks with weight losses at around 80, 170, 380, and 500 °C, respectively (Figure 5). The endothermic peaks below 100 °C correspond to the evaporation of adsorbed water, and the peak at around 170 °C corresponds to the loss of water by condensation of the lattice −OH groups of the spinel structure. The −OH groups are formed by Li^+/H^+ and Zn^{2+}/H^+ ion-exchange extraction reactions. The peaks at around 380 and 500 °C can be ascribed to the transformation from tetravalent manganese to trivalent manganese accompanying the loss of oxygen gas.

An endothermic peak at around 160 °C and a shoulder at around 210 °C with weight losses were observed for the lattice −OH groups in the DTA-TG curves of sample Zn-400(H) (Figure 5). This suggests the presence of two kinds of lattice −OH groups. The lattice −OH groups are formed by the ion-exchange reaction of Li^+ and Zn^{2+} in both the tetrahedral and octahedral sites with protons. The protonated octahedral site may be more unstable than the protonated tetrahedral site, because the vacancy is larger at the octahedral site than at the

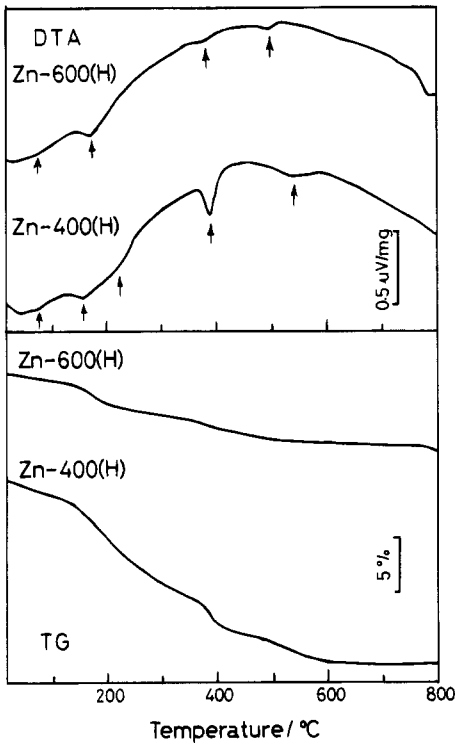

Figure 5. DTA (top) and TG (bottom) curves for the acid-treated samples.

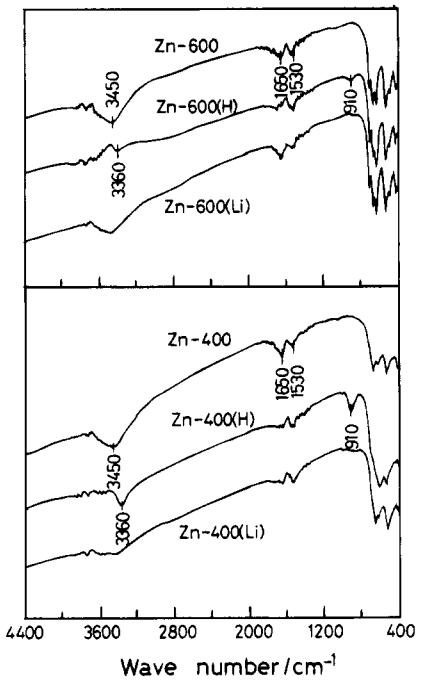

Figure 6. IR spectra of the original, acid-treated, and Li^+-inserted samples.

tetrahedral site. The endothermic peak at the lower temperature, therefore, can be assigned to the protons at octahedral sites. The lattice proton contents (H/Mn) were evaluated from the the weight loss between 120 and 300 °C, as is shown in Table 1.

IR spectra of the original, acid-treated, and Li^+-inserted samples are shown in Figure 6. The spectra of the original samples show absorption bands at 3450 and 1650 cm^{-1}, corresponding to the vibrations of adsorbed water. The bands in the region from 400 to 800 cm^{-1} can be assigned to Mn−O and Zn−O stretching vibrations. More vibration modes of Mn−O and Zn−O were observed in the spectrum of Zn-600 than in that of Zn-400, owing to cation ordering in Zn-600 spinel.[29] The bands at 3360 and 910 cm^{-1} in the acid-treated samples (Zn-600(H) and Zn-400(H)) can be assigned to the stretching vibration of the lattice −OH group and lattice coupling vibration of the H^+-form spinel, respectively.[10] Similar bands were also observed in the spectra of acid-treated $Li_{1.33}Mn_{1.67}O_4$,[22] $LiMg_{0.5}MnO_4$,[24] and $LiFeMnO_4$[25] spinels where Li^+ is extracted by ion-exchange reactions but not observed in that of acid-treated $LiMn_2O_4$ spinel[22] where Li^+ is extracted by a redox-type reaction.

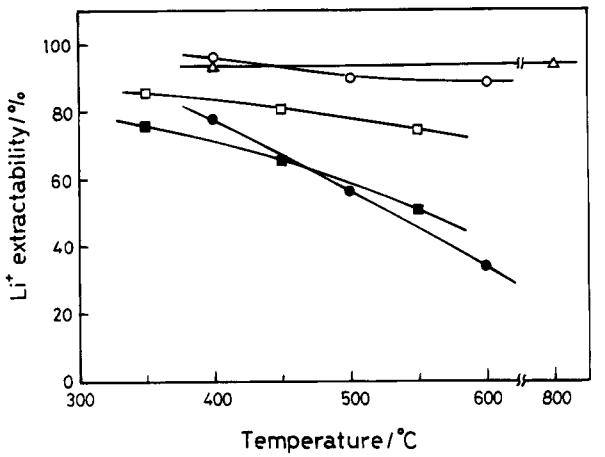

Figure 7. Effect of heat-treatment temperature on the Li^+ extractabilities by acid treatment (1 M HNO_3 solution) for $(Li_{0.5}Zn_{0.5})[Li_{0.5}Mn_{1.5}]O_4$ (●), $(Li)[Mg_{0.5}Mn_{1.5}]O_4$ (○),[23] $(Li_{0.6}Fe_{0.4})[Li_{0.4}Fe_{0.6}Mn]O_4$ (■),[24] $(Li)[AlMn]O_4$ (□),[24] and $(Li)[Li_xMn_{2-y}]O_4$ (△)[21] spinel systems.

Effect of Cation Arrangement on Li^+ Extraction. The Li^+ extractabilities for various spinel systems are summarized in Figure 7 as a function of the heat-treatment temperature. The spinel systems with bivalent or trivalent metal cations at the 8a tetrahedral sites ($(Li_{0.5}Zn_{0.5})[Li_{0.5}Mn_{1.5}]O_4$ and $(Li_{0.6}Fe_{0.4})[Li_{0.4}Fe_{0.6}Mn]O_4$[25]) show a lower Li^+ extractability and larger temperature dependence than those with Li^+ alone at tetrahedral sites ($(Li)[Mg_{0.5}Mn_{1.5}]O_4$,[24] $(Li)[AlMn]O_4$,[25] and $(Li)[Li_xMn_{2-y}]O_4$[22]). This suggests that the Li^+ extraction reaction is influenced by the cation distribution in the spinel.

The Li^+ extraction reaction proceeds by the migration of Li^+ from the bulk crystal to the crystal surface through the three-dimensional tunnels of the spinel structure. The three-dimensional tunnels are constituted of interconnected interstitial space of 8a tetrahedral sites and empty 16c octahedral sites in the cubic closed-packed oxygen framework.[1] The tunnel is directed from an 8a tetrahedral site toward its nearest-neighboring four 8a tetrahedral sites. In the spinel with empty 8a sites or Li^+ alone at the 8a sites, Li^+ can migrate from the bulk crystal to the surface through 8a → 16c → 8a → 16c pathways for Li^+ at 8a tetrahedral sites or 16d → 16c → 8a → 16c → 8a pathways for Li^+ at 16d octahedral sites. But when the 8a tetrahedral sites are occupied by immobile or lower mobility metal cations, for example, bivalent or trivalent metal cations, the Li^+ migration may be inhibited by these cations.

(29) Gryffroy, D.; Vandenberghe, R. E. *J. Phys. Chem. Solids* **1992**, *53*, 777.

Studies on Li^+ conductors of ternary lithium chloride spinels Li_2MCl_4 have indicated that the $(Zn)[Li_2]Cl_4$ spinel shows a lower Li^+ conductivity and a higher activation energy than $(Li)[LiM]Cl_4$ (M = Mg, Mn, Cd, V) spinels.[30-35] Li^+ conductivities of the $(Li)[Li_{1-x}NaxM]Cl_4$ (M = Mn, Cd) spinels decrease only slightly with an increase in sodium content, but the conductivities of $(Li_{1-x}Cu_x)[LiM]Cl_4$ spinels strongly decrease with an increase in copper content.[30] These facts suggest that Li^+ at 8a tetrahedral sites show higher mobility than those at 16d octahedral sites, and the metal ions at the tetrahedral sites inhibit Li^+ migration. We think that the mechanism of Li^+ migration in the oxide spinels is similar to that in the lithium chloride spinels.

The remarkable decrease of Li^+ extractability with an increase in heating temperature for the $(Li_{0.5}Zn_{0.5})[Li_{0.5}Mn_{1.5}]O_4$ spinel system (Figure 7) may be due to the tendency for the ordered arrangement of Li^+ and Zn^{2+} at 8a sites to increase and Zn^{2+} extractability to decrease with increasing heating temperature. In the spinel with the ordered arrangement (Zn-600), all four nearest-neighboring 8a sites of any Li^+ at 8a site are occupied by Zn^{2+} (Figure 2). Namely, all the 8a → 16c → 8a → 16c pathways for the Li^+ migration are blocked by ordered Zn^{2+} ions. Although Li^+ migration through Li^+-occupied 8a → 16c → Li^+-occupied 16d → 16c → Li^+-occupied 8a pathway may be also possible, it is more difficult than that through the 8a → 16c → 8a → 16c tunnel. Li^+ suffers an electrostatic repulsion from Zn^{2+} at 8a sites when it enters 16c sites. In the randomly arranged spinel (Zn-400), however, not all the pathways for Li^+ migration are blocked by Zn^{2+}, unlike the case in the ordered spinel (Zn-600).

Li^+ Insertion from LiOH Solution. X-ray diffraction patterns of the Li^+-inserted samples (Zn-600)(Li) and Zn-400(Li)) show that the spinel structures remained after Li^+ insertion (Figure 4, bottom), indicating that the Li^+ insertion reaction is a topotactic reaction. The IR spectra show that the vibration bands (910 and 3360 cm^{-1}) corresponding to the lattice −OH group decrease in intensity with Li^+ insertion (Figure 6), owing to a H^+/Li^+ ion-exchange reaction.

The compositional analysis results for the Li^+-inserted samples are given in Table 1. The lattice proton contents decrease with Li^+ insertion by an ion-exchange mechanism. The lattice protons, however, cannot be fully exchanged by Li^+ even in a 0.1 M LiOH solution, similar to the cases of acid-treated $Li_{1.33}Mn_{1.67}O_4$, $LiMg_{0.5}Mn_{1.5}O_4$, $LiAlMnO_4$, and $LiFeMnO_4$ spinels.[22,24,25] This may be due to the fact that the two different kinds of lattice protons (one located at 8a tetrahedral sites and the other at 16d octahedral sites) show different ion-exchange properties for Li^+. The DTA-TG analysis study indicates that the endothermic peak at around 210 °C for Zn-400(H) (Figure 5), which can be ascribed to the lattice proton at tetrahedral sites, disappears on Li^+ insertion. However, the peaks at around 170 °C for Zn-600(H) and 160 °C for Zn-400(H), which can be ascribed to the lattice proton at octahedral sites, remain but shift to higher temperatures (195 and 185 °C, respectively) after the Li^+ insertions. This suggests that the lattice protons at the tetrahedral sites are more easily exchanged with Li^+ than those at the octahedral sites. Since the tetrahedral sites are located on the pathway of Li^+ migration, Li^+ insertion into the tetrahedral site is easier than that into the octahedral site.

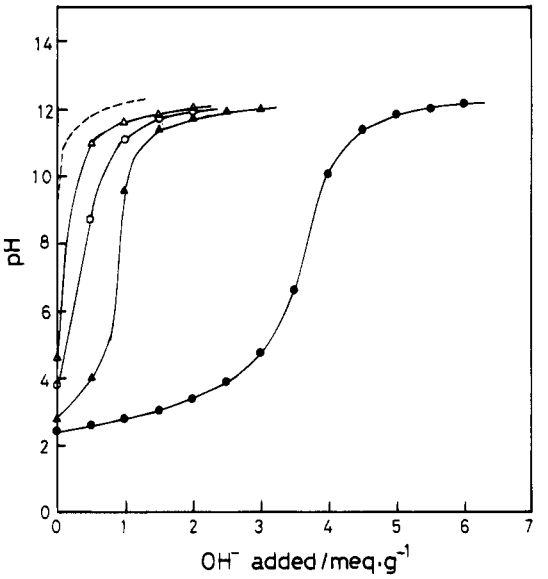

Figure 8. pH titration curves of the acid-treated samples. Sample, 0.100 g; solution (0.1 M MCl + MOH: M = Li (solid marks) or Na (open marks)); total volume of solution, 10 mL; temperature, 20 °C. (▲, △), Zn-600(H); (●, ○), Zn-400(H); (– – –) blank titration.

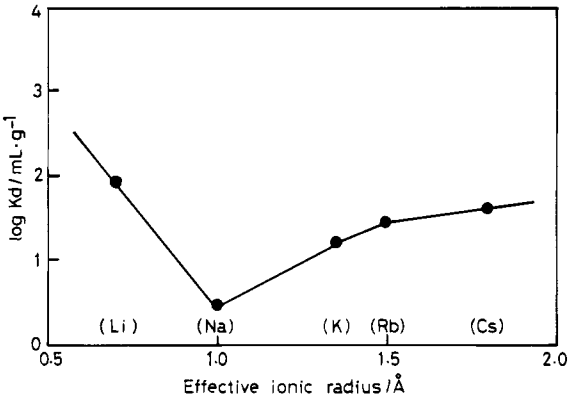

Figure 9. Distribution coefficients of alkali-metal ions on Zn-400(H) at pH 2 and 20 °C as a function of effective ionic radius.

Adsorptive Properties for Alkali-Metal Ions. The pH titration curves of the acid-treated samples (Zn-600(H) and Zn-400(H)) toward Li^+ and Na^+ are given in Figure 8. Both samples show lithium ion-sieve properties; the apparent capacities for Li^+ are significantly larger than those for Na^+ over the pH range studied. This indicates that Li^+ is exchangeable with the lattice proton in the bulk crystal, while Na^+ is not exchangeable with the lattice proton but only exchangeable with the surface proton which is nonspecific for metal ions.[12,22,23] The apparent capacity of Zn-600(H) for Li^+ is remarkably smaller than that of Zn-400(H),

(30) Lutz, H. D.; Kuske, P.; Wussow, K. *Solid State Ionics* **1988**, *28–30*, 1282.
(31) Lutz, H. D.; Schmidt, W.; Haeuseler, H. *J. Phys. Chem. Solids* 1981, *42*, 287.
(32) Kanno, R.; Takeda, Y.; Yamamoto, O. *Mater. Res. Bull.* **1981**, *16*, 999.
(33) Kanno, R.; Takeda, Y.; Takata, K.; Yamamoto, O. *J. Electrochem. Soc.* **1984**, *131*, 469.
(34) Kanno, R.; Takeda, Y.; Yamamoto, O. *Solid State Ionics* **1988**, *28–30*, 1276.
(35) Soubeyroux, J. L.; Cros, C.; Gang, W.; Kanno, R.; Pouchard, M. *Solid State Ionics* **1985**, *15*, 293.
(36) Shannon, R. D.; Prewitt, C. T. *Acta Crystallogr.* **1969**, *B25*, 925.

owing to a lower content of lattice protons at tetrahedral sites in Zn-600(H).

The equilibrium distribution coefficients (Kd) of alkali-metal ions on the Zn-400(H) sample were measured at pH 2. The log K_d values are plotted as a function of the effective ionic radii[36] of the alkali metal ions in Figure 9. The selectivity sequence for the alkali metal ions is $Na^+ < K^+ < Rb^+ < Cs^+ < Li^+$, showing a specific selectivity for the adsorption of Li^+. The high selectivity for Li^+ can be explained by the ion-sieve effect of the spinel lattice.[10,12,14] The Li^+ with its smaller ionic radius can enter the spinel lattice after dehydration and exchange with the lattice protons in the bulk crystal, impossible for other alkali-metal ions because their ionic radii are too large. These ions exchange with surface protons alone in hydrated forms, which gives a selectivity sequence, increasing with the decrease of hydrated radii.

Conclusions

Lithium–zinc–manganese oxide spinels with a cation distribution of $(Li_{0.5}Zn_{0.5})[Li_{0.5}Mn_{1.5}]O_4$ are prepared by a coprecipitation/thermal crystallization method. The Li^+ extraction/insertion reactions with the spinels proceed by topotactic ion-exchange-type mechanisms. Zn^{2+} at 8a tetrahedral sites inhibit Li^+ extraction from the spinels. The inhibiting effect becomes more notable for the spinel with ordered arrangement of Li^+ and Zn^{2+} at the tetrahedral sites. The Li^+-extracted sample shows a lithium ion-sieve property.

CM940430M